PHYSICAL REVIEW A

GENERAL PHYSICS

THIRD SERIES, VOLUME 36, NUMBER 3 AUGUST 1, 1987

Excitation of the $1s_5$ and $1s_4$ levels of neon by low-energy electrons

K. Tachibana

*Joint Institute for Laboratory Astrophysics, National Bureau of Standards and University of Colorado, Boulder, Colorado 80309-0440 and Department of Electronics, Kyoto Institute of Technology, Matsugasaki, Sakyo-ku, Kyoto 606, Japan**

A. V. Phelps†

Joint Institute for Laboratory Astrophysics, National Bureau of Standards and University of Colorado, Boulder, Colorado 80309-0440

(Received 24 February 1987)

Excitation coefficients for production of $1s_5$ and $1s_4$ levels (Paschen notation) of neon in collisions with low-energy electrons have been measured using a drift-tube technique combined with laser absorption and laser-induced fluorescence techniques. The absorption and fluorescence signals have been analyzed using coupled rate equations which include the effects of population mixing among these levels in collisions with neon atoms. The excitation coefficients for the metastable and resonance levels α_M/N and α_R/N have been obtained as functions of the electric field to gas density ratio E/N. The measured values of α_M/N vary from 1.3×10^{-24} m^2 at $E/N=1.6\times10^{-21}$ V m^2 to 6.5×10^{-22} m^2 at 3.0×10^{-19} V m^2. The values of α_R/N are comparable in the experimental E/N range. The experimental excitation coefficients are in agreement with values calculated from a Boltzmann analysis using a recommended set of electron excitation cross sections derived from published experimental electron beam data.

I. INTRODUCTION

This paper presents measurements and analyses of swarm coefficients for the electron excitation of the two lowest excited states of neon, i.e., the $1s_5$ and $1s_4$ levels (Paschen notation[1]). This is the second in a series of papers on the use of drift-tube techniques and Boltzmann analysis for the determination of the excitation coefficients and cross sections for the levels of rare-gas atoms in the lowest electronic configuration. In the first of the series,[2] one of the present authors (K.T.) has recently reported on the excitation of argon. The reporting of the neon data was delayed[3] pending an analysis of the effects of collisional mixing, of Penning ionization of impurities, and the determination of a consistent set of electron excitation cross sections. The derived excitation coefficients are compared with values calculated from solutions of the Boltzmann equation using cross sections chosen from among published experimental[4,5] and theoretical[6] results. A recommended set of elastic and inelastic cross sections is presented which reproduces the measured excitation coefficients and published transport and ionization coefficients to within their respective estimated uncertainties. The only other application of absorption techniques to the measurement of neon excitation appears to be that of Milatz and Ornstein.[7] Laser-induced fluorescence techniques were recently used to measure cross sections for excitation of the four $1s$ levels of neon.[4]

The approach used in these determinations of excitation coefficients is to first determine the absolute excited-state density from measurements of the fractional adsorption of monochromatic radiation and from previously reported determinations of the relevant radiative transition probabilities. Determination of the excited-state lifetimes then allows us to calculate the rate of loss of excited atoms, which is equal to the steady-state production rate by swarm electrons. A particularly important improvement in the present series of experiments over previous neon metastable absorption experiments is the use of a narrow-band laser to measure both the magnitude of the absorption at the line center and the shape of the absorption profile.

In Sec. II we review briefly the experimental apparatus and technique, while in Sec. III we present the new aspects of the theory of the experiment. The experimental results are presented in Sec. IV and the Boltzmann analysis relating the electron collision cross sections to the measured excitation coefficients is summarized in Sec. V. Section VI presents a discussion of various factors affecting the accuracy and interpretation of the results.

II. EXPERIMENTAL APPARATUS AND PROCEDURE

The experimental setup is shown schematically in Fig. 1. Since the apparatus and the procedure are almost the same as those for the experiments with argon (see Ref. 2)

 ©1987 The American Physical Society

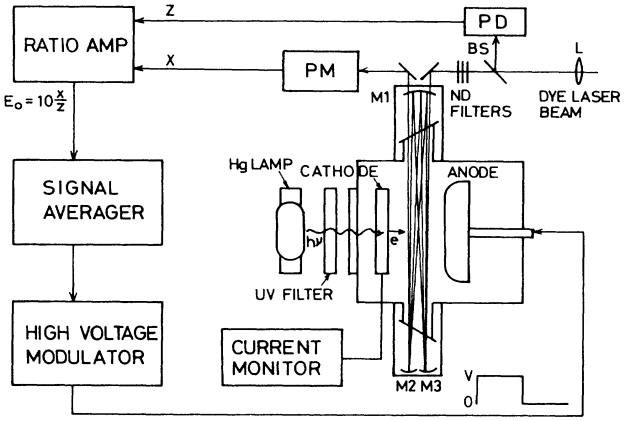

FIG. 1. Schematic of the experimental setup.

we will cite this reference for some details and will refer to it as I. The drift tube is the same one used for the experiments[8] with O_2. The diameter of the semitransparent photocathode was 60 mm and the electrode separation L was 38.4 mm. The photocathode was uniformly illuminated from outside the vacuum chamber with a 100-W mercury lamp which had been removed from its uv-absorbing envelope. Research grade neon (99.995% nominal purity) was used. Before filling the system, the neon was cooled in a liquid-N_2 trap for about an hour to remove water vapor.[9] The filling pressure ranged from 40 to 4000 Pa. The E/N range studied was 1.6×10^{-21} to 3.0×10^{-19} V m^2 as produced by a square-wave accelerating voltage of 50–150 V. These voltages were well below breakdown. The electrons were produced in significant numbers at the cathode only by the external illumination and not by metastables or neon resonance photons arriving at the cathode. The light source for the absorption and fluorescence measurements was a single-mode dye laser pumped by an argon-ion laser. The linewidth was estimated to be less than a few tens of megahurtz. The wavelength of the laser was locked to the center of the absorption line using the optogalvanic signal from a commercial hollow-cathode lamp to generate an error signal. The resultant frequency stability was better than ±100 MHz.

The absorption measurements were made using a multipass optical configuration in which the folded laser beam was in a plane which included the axis of the drift tube. The beam crossed the tube axis at positions from $z_1=6.5$ mm to $z_2=32$ mm, where the cathode surface is taken to be at $z=0$. The number of passes could be adjusted from 32 to 40 corresponding to absorption lengths in the active drift region of from 1.92 to 2.4 m. Proper adjustment of the mirrors resulted in a uniform distribution of the laser beams throughout the region from z_1 to z_2 so that the fractional absorption was equal to the product of the absorption coefficient at the laser frequency,[2] the path length, and the average excited-state density in the region between z_1 and z_2. The beam diameter in the active region was about 1 mm and the laser intensity was attenuated to about 10^{-4} mW/mm^2, which is well below the experimentally determined value of 10^{-2} mW/mm^2 at which pumping by the laser perturbs the excited-state density. A ratio amplifier was used to compensate for fluctuations in the laser power. The number of sweeps used for signal averaging was 10^3 to 2×10^4 and the resultant rms noise corresponded to about 0.01% absorption or a minimum detectable density of 10^{11} m^{-3}. Linearity of the detection system was checked by observing the absorption signal while varying the dye laser intensity from 10^{-5} to 10^{-3} mW/mm^2.

The transitions at wavelengths of 588.2, 594.5, and 614.3 nm were used to determine the $1s_5$ density. The densities of $1s_5$ atoms obtained using the three lines agree with each other to within experimental scatter when the transition probabilities[10] of Bridges and Wiese or of Inatsugu and Holmes are used. The 609.6-nm line was used for the $1s_4$ level. Figure 2 shows representative absorption transients obtained using the 614.3- and 609.6-nm lines. The fitting of these data to theory and the use

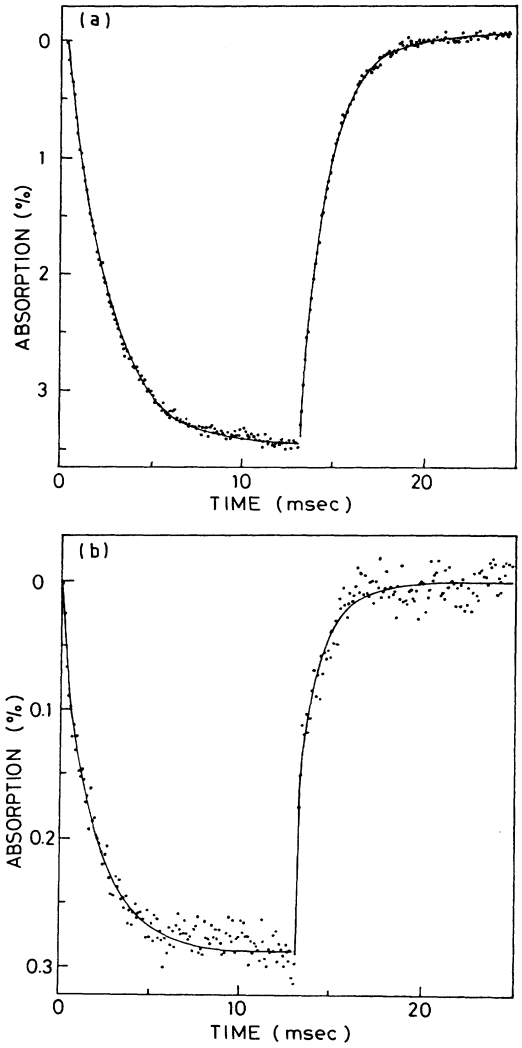

FIG. 2. Examples of the transient absorption signals for (a) the $1s_5$ level and (b) the $1s_4$ level as measured using the wavelengths 614.3 and 609.6 nm, respectively. Here $E/N=2\times10^{-20}$ V m^2 and $N=1.93\times10^{23}$ m^{-3}.

of the data will be discussed in Sec. IV.

A fluorescence technique was also employed for time constant and relative density measurements for the $1s_5$ level because it is more sensitive than the absorption technique. All of the fluorescence measurements of transient excited-state densities reported here were made using laser excitation at 588.2 nm and detection of 659.9-nm emission using an interference filter. In this case the multipass optical configuration was replaced with a single-pass configuration with an expanded laser beam diameter of 30 mm. This allowed an increase in the laser power while keeping the laser intensity below 10^{-3} mW/mm^2 so as to avoid pumping effects. Thus our conditions are much different from those of the laser-induced fluorescence experiments of Ref. 4. The detector was placed to observe the fluorescence at right angles to the laser beam. The multichannel scalar was operated in the pulse counting mode. The relative fluorescence signals were converted to absolute excited-state densities by comparison with values obtained from the absorption measurements at $E/N=1\times10^{-20}$ V m^2 In order to avoid making corrections for the density dependences of collisional quenching,[11] etc. of the $2p$ levels, the fluorescence measurements were made at fixed gas density and variable voltage and were normalized at overlapping E/N. The fluorescence technique was not used for the $1s_4$ level since it was difficult to distinguish the rapidly varying fluorescence signal from the emission resulting from electron excitation of the upper level (see Fig. 2).

The profiles of the lines used in these experiments were measured using the fluorescence technique in which the laser was scanned in wavelength. Thus, at low Ne densities the profile of the 588.2-nm line was consistent with two Doppler-broadened components having the measured fractional natural abundance of ^{22}Ne and the reported[12] isotope shift of 1.75 GHz. At the higher Ne densities, the lineshapes were consistent with the published[13,14] values for the collision broadening coefficients of 3.4×10^{-25} GHz m^3 for the 588.2-, 594.5-, and 614.3-nm lines and 3.2×10^{-25} GHz m^3 for the 609.6-nm line. These results were taken into account in the derivation of excited-state densities from the absorption signals.

III. THEORY OF EXPERIMENT

In this section we will present a derivation of the expressions for the excitation coefficients in terms of the measured average excited-state densities and decay constants. Although some modifications in the procedure of date analysis used for argon are necessary for neon, the procedure is similar to that given in I. The model of the excited-state afterglow processes is a simplified version of that of Phelps,[15] while the treatments of excited-state diffusion, spatially dependent detection efficiency, etc., are similar to those developed for O_2 metastables.[8] The rate equations for the $1s_5$ and $1s_4$ levels are

$$\frac{\partial M(z,t)}{\partial t}=k_M N n_e(0,t)e^{\alpha_i z}+\frac{D\partial^2 M}{\partial z^2}-(K_1N+K'_MN+K_{2M}N^2)M+aK_1NR\ . \quad (1)$$

$$\frac{\partial R(z,t)}{\partial t}=k_R N n_e(0,t)e^{\alpha_i z}-(\nu_I+aK_1N+K'_RN+K_{2R}N^2)R+K_1NM\ , \quad (2)$$

where $M(z,t)$ and $R(z,t)$ are the spatial- and time-dependent densities of the $1s_5$ and $1s_4$ levels, k_M and k_R are the respective electron excitation rate coefficients, $n_e(0,t)$ is the density of photoelectrons at the cathode, α_i is the spatial ionization coefficient characterizing the exponential growth of the electron density, N is the neon atom density, D is the diffusion coefficient for the $1s_5$ atoms, ν_I is the effective radiative transition probability for the $1s_4$ level including the effects of radiation trapping,[2,15] K_1 is the rate coefficient for excitation transfer from $1s_5$ to $1s_4$, $a=12.4$ is the equilibrium ratio of $1s_5$ to $1s_4$ densities at 300 K, K_{2M} and K_{2R} are the rate coefficients for three-body collisional quenching, and K'_M and K'_R are the effective rate coefficients for $1s_5$ and $1s_4$ state quenching by impurities. These equations are the same as Eqs. (2) and (3) of I except that the terms aK_1NR and K_1NM have been added to include collisional mixing of these levels and the terms in K'_M and K'_R have been added to account for quenching by impurities. Note that we have very much simplified the treatment of the transport of the resonance radiation emitted by the $1s_4$ level by replacing the Holstein-Biberman integrals by a constant ν_I characteristic of the fundamental decay mode[16] as calculated using the measured $1s_4$ radiative lifetime.[17] An empirical justification for this approximation has been given in the case of the theory of electrical breakdown of rare gases.[18] In Eqs. (1) and (2) the electron density is assumed to be given by the quasi-steady-state solution,[2,8] i.e., by $n_e(z,t)=n_e(0,t)\exp(\alpha_i z)$. The boundary conditions appropriate to Eq. (1) are that $M(0)=0$ and $M(L)=0$, where L is the separation of the electrodes. $R(0)$ and $R(L)$ are finite in this model.

The general approach used for the solution of Eqs. (1) and (2) is to make a Fourier-series expansion of the spatial dependence of M and R, e.g., $M(z,t)=\sum_m f_m(t)\sin(m\pi z/L)$. For each m one then obtains two coupled rate equations having two characteristic decay constants. We are primarily concerned with the resulting steady-state solution and the slow or final decay constant of the lowest spatial mode ($m=1$). The steady-state solutions are

$$M(z)=n_e(0)N(k_M\omega_0+k_RaK_1N)\sum_m\frac{b_m\sin(m\pi z/L)}{[\gamma_m\omega_0-a(K_1N)^2]}=\frac{n_e(0)N[k_M\omega_0+k_RaK_1N]}{\nu^2}[e^{\alpha_i z}-F(z)]\ , \quad (3)$$

$$R(z)=\frac{n_e(0)N}{\nu^2}\left[[k_R(\gamma_0-\alpha_i^2D)+k_MK_1N]e^{\alpha_i z}-\left[\frac{k_Ra(K_1N)^2}{\omega_0}+k_MK_1N\right]F(z)\right]\ , \quad (4)$$

where

$$\nu^2=\gamma_0\omega_0-a(K_1N)^2-\alpha_i^2D\omega_0 , \tag{5}$$

$$F(z)=[\sinh(h\pi)]^{-1}\{\sinh[h\pi(1-z/L)] + e^{\alpha_iL}\sinh(h\pi z/L)\} , \tag{6}$$

$$h^2=\left[\frac{L}{\pi}\right]^2\frac{[\gamma_0\omega_0-a(K_1N)^2]}{D\omega_0} . \tag{7}$$

Here $\gamma_0=K_1N+K_M'N+K_{2M}N^2$, $\omega_0=\nu_1+aK_1N+K_R'N+K_{2R}N^2$, $\gamma_m=D(m\pi/L)^2+\gamma_0$, and $b_m=2\pi m[1-(-1)^me^{\alpha_iL}]/[(\alpha_iL)^2+(m\pi)^2]$.

Since the absorption measurements yield the average $1s_5$ and $1s_4$ atom densities M_s and R_s in the region from z_1 to $z_2=L-z_1$, we wish to evaluate these quantities from Eqs. (3) and (4). The results are

$$M_s=\frac{n_e(L)N}{\nu^2Q(z_2,z_1)}(k_M\omega_0+k_RaK_1N)H(z_2,z_1) , \tag{8}$$

$$R_s=\frac{n_e(L)N}{\nu^2Q(z_2,z_1)}(k_R\gamma_1P+k_MK_1N)H(z_2,z_1) , \tag{9}$$

$$H(z_2,z_1)=1-\frac{\alpha_iL(e^{\alpha_iL}+1)}{(e^{\alpha_iz_2}-e^{\alpha_iz_1})}\frac{\sinh[h\pi(z_2-z_1)/2L]}{h\pi\cosh[h\pi/2]}, \tag{10}$$

$$P=[\gamma_0\omega_0-\alpha_i^2D\omega_0-a(K_1N)^2(1-H)](\gamma_1\omega_0H)^{-1} , \tag{11}$$

$$\gamma_1=\gamma_0+D(\pi/L)^2 , \tag{12}$$

$$Q(z_2,z_1)=\alpha_i(z_2-z_1)e^{\alpha_iL}(e^{\alpha_iz_2}-e^{\alpha_iz_1})^{-1} . \tag{13}$$

Note that the use of γ_1 rather than γ_0 in Eqs. (9) and (11) is optional and was chosen because the resultant geometrical factor P defined by Eq. (11) then varies only from 0.93 at low N (high E/N) to 1 at high N (low E/N). The factor Q accounts for the growth of electron density and replaces the factor q used in previous papers.[2,8]

In the case of absorption measurements at the center of the drift region, i.e., when $z_1=z_2=L/2$ as in I, the quantities H and Q reduce to

$$H=1-\cosh(\alpha_iL/2)\mathrm{sech}(h\pi/2) , \tag{10'}$$

$$Q=e^{\alpha_iL/2} . \tag{13'}$$

In the limit of $K_1=0$ these expressions can be shown to lead to those given for M_s and R_s in I.

The final expressions for the excitation coefficients are obtained by solving Eqs. (8) and (9) for k_M and k_R and noting that $\alpha_M/N=k_M/w_e$, $\alpha_R/N=k_R/w_e$, and $i=Aew_en_e(0)\exp(\alpha_iL)$. Here w_e is the electron drift velocity, e is the electronic charge, i is the total current at the anode, and A is the cathode area. The resultant equations are

$$\frac{\alpha_M}{N}=AeQ\left[\frac{M_s}{iN}\right][\gamma_1P-aK_1N(R_s/M_3)] , \tag{14}$$

$$\frac{\alpha_R}{N}=AeQ\left[\frac{R_s}{iN}\right][\omega_0-K_1N(M_s/R_s)] . \tag{15}$$

Equations (14) and (15) show that in addition to the magnitudes of the average excited-state densities M_s and R_s, the determinations of α_M/N and α_R/N require a knowledge of the frequencies γ_1 and ω_0, the rate coefficient K_1, and the ionization coefficient α_i. Our general approach is to use collisional rate coefficients consistent with previous measurements in pure Ne, but with K_M' and K_R' adjusted to allow for the effects of impurities which appear to have been present in our gas samples. Details are discussed in Sec. IV. As discussed in earlier papers,[2,8] the final decay of the excited-state density is exponential with a decay constant determined by the lowest spatial diffusion mode, i.e., by

$$\gamma_f=0.5\{(\gamma_1+\omega_0)-[(\omega_0-\gamma_1)^2+4a(K_1N)^2]^{1/2}\} . \tag{16}$$

The corresponding fast or initial decay constant is given by

$$\gamma_i=0.5\{(\gamma_1+\omega_0)+[(\omega_0-\gamma_1)^2+4a(K_1N)^2]^{1/2}\} . \tag{17}$$

Because ω_0 is large compared to $D(\pi/L)^2$ at neon densities of interest here, the value of γ_i is insensitive to the assumption of the lowest diffusion mode and it is useful to approximate the time dependences of the $1s_5$ and $1s_4$ densities by

$$M(t)-A_1e^{-\gamma_it}+A_2e^{-\gamma_ft}+A_3 \tag{18}$$

and

$$R(t)=B_1e^{-\gamma_it}+B_2e^{-\gamma_ft}+B_3 . \tag{19}$$

The usefulness of the fundamental diffusion mode approximation made in Eqs. (16) through (19) is discussed in detail in Ref. 8 for O_2 metastables.

IV. EXPERIMENTAL RESULTS

Typical absorption signals for the $1s_5$ and $1s_4$ levels are shown by the points in Figs. 2(a) and 2(b), respectively. The two sets of absorption data were obtained at the same E/N and N values. The solid curves in Figs. 2(a) and 2(b) are least-squares fits of Eqs. (18) and (19), respectively. The waveform in the decay period for the $1s_5$ level can be fitted by a single exponential function of time. This means that the contribution of the first term in Eq. (19) is negligibly small. On the other hand, the waveform for the $1s_4$ level appears to be a double exponential function of time. The initial decay constant γ_i, however, is of questionable accuracy because of the finite response time of our measuring system.

The final decay constants γ_f obtained from such data are shown by the points in Fig. 3 as a function of the gas density. The circle points are from absorption data and the square points are from fluorescence data. As expected from the theory of Sec. III, the values of γ_f for the $1s_4$ level (open circles) agree with those for the $1s_5$ level (solid circles) to within the scatter of the data. The dashed curve in Fig. 3 shows the least-squares fit to the experimental data of Eq. (16) in which $K_M'=K_R'=0$, as in pure Ne, and in which DN and K_1 were varied. The constants used in the fit are $DN=6.2\times10^{20}$ $\mathrm{m^{-1}\,s^{-1}}$, $K_1=4.9\times10^{-21}$ $\mathrm{m^3\,s^{-1}}$, $\nu_1=1.43\times10^4$ $\mathrm{s^{-1}}$, $K_{2M}=5.0\times10^{-46}$ $\mathrm{m^6\,s^{-1}}$, and $K_{2R}=5.0\times10^{-45}$ $\mathrm{m^6\,s^{-1}}$. Here ν_1 was calculated from Eq. (16) of I using the report-

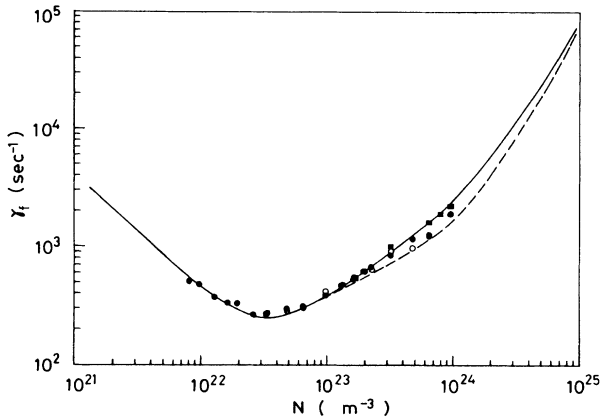

FIG. 3. Dependence of the final decay constant γ_f on gas density N from measurements of the $1s_5$ density transient by absorption (●) and by fluorescence (■) and for the $1s_4$ level by absorption (○). The solid and dashed curves show the calculated values with and without the destruction by impurities, respectively.

ed radiative lifetime.[17] The values for K_{2M} and K_{2R} were taken from Refs. 15 and 19, respectively, because our pressure range was not large enough for their determination. It should be noted that the value of K_1 determined here is somewhat larger than previously reported values.[15,19,20] Even more important is the poor fit of the calculated values of γ_f with the measured values at the higher N.

A better fit of the calculated and measured γ_f values is obtained if we introduce quenching of the $1s_5$ and $1s_4$ levels by collisions with impurity atoms or molecules. From Eqs. (1) and (2), K'_M and K'_R are the apparent rate coefficients for the quenching of the $1s_5$ and $1s_4$ atoms by impurities and are the products of the actual quenching rate coefficients and the fractional concentration of the impurity. The solid curve of Fig. 3 shows the fit to the fluorescence data. This data was selected for emphasis because of its better signal to noise at late times and because it was obtained in a short period of time. Here the values of K'_M and K'_R from the fit are 8×10^{-22} and 4×10^{-21} m^3 s^{-1}, respectively. In this fit we used the published value[15] of $K_1=3.4\times10^{-21}$ m^3 s^{-1} and modified K_{2M} to 4×10^{-46} m^6 s^{-1}. The values of K'_M and K'_R imply that the impurity concentration is 10 to 100 ppm if the quenching rate coefficient[21] is 10^{-17} to 10^{-16} m^3 s^{-1}. This impurity level is consistent with the manufacturer's specifications for the neon gas samples used. As indicated by the scatter of the data of Fig. 3, many of the final decay constants obtained from the absorption transients are more accurately fit by lower effective rate coefficients for quenching by impurities than those found for the fluorescence data. Therefore, the values of K'_M and K'_R used with the absorption data were scaled from the values obtained with the fluorescence data by an impurity level factor so as to fit the measurement of γ_f which was concurrent with the M_s or R_s determination.

Since the effort required to change the laser frequency from one line to another precluded simultaneous measurements of the $1s_5$ and $1s_4$ absorption transients, we have compared steady-state data from a number of different runs to obtain the values of R_s/M_s versus N shown in Fig. 4. The R_s/M_s values for different E/N are indicated by different symbols, but no systematic dependence on E/N is evident. A smooth curve is drawn through the points and values from this curve were used in Eqs. (14) and (15). Note that the R_s/M_s values approach the thermal equilibrium limit at the higher N.

Also shown in Fig. 4 are experimental values (solid circles) of the ratio of $1s_5$ and $1s_4$ densities R_f/M_f during the final decay following the removal of electron excitation. The experimental data are in better agreement with the calculated values when quenching by impurities (solid curve) is included than when impurity effects are omitted (dashed curve). Although not as good as in previous investigations,[15] this agreement with the model is considered satisfactory.

The values of the excitation coefficient for the $1s_5$ level, α_M/N, obtained from Eq. (14) using the measured values of M_s/iN, R_s/iN, R_s/M_s, and the rate coefficients obtained by fitting γ_f data, are shown in Fig. 5. The values deduced from the absorption measurements are shown by the open circles and are averages of data obtained at a particular E/N. The relative values from the fluorescence measurements, shown by the solid circles, have been placed on an absolute scale by comparison with the values from absorption data at $E/N=10^{-20}$ V m^2. The values of the excitation coefficient for the $1s_4$ level, α_R/N, obtained from Eq. (15), are shown by the circles in Fig. 6. The solid curves in both figures show the values for direct excitation as calculated from the Boltzmann analysis using the recommended cross-section set discussed in Sec. V. At the lower E/N our measured values of α_M/N agree very well with the calculated values shown in Fig. 5. At the higher E/N, however, the measured values are much larger than indicated by the solid curve. This difference is attributed to the cascading to the $1s$ levels from higher-lying levels such as the $2p$ levels. We can calculate the cascade contributions for the various $1s$ lev-

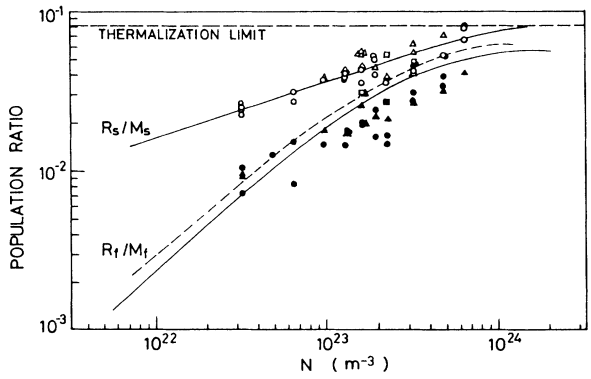

FIG. 4. Dependences of the ratios of $1s_5$ density to $1s_4$ density in the steady-state R_s/M_s and in the late afterglow R_f/M_f on Ne density N. The solid and dashed curves for R_f/M_f are with and without impurity effects, respectively. The solid curve for R_s/M_s is a smooth fit to the data. The thermalization limit is for collisional equilibrium at 300 K.

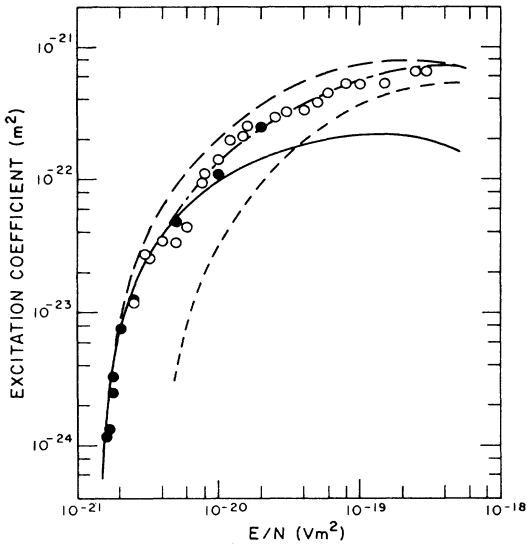

FIG. 5. Excitation coefficients α_M/N for the $1s_5$ level as a function of E/N. The open circles are from absorption data, while the solid circles are from normalized fluorescence data. The solid curve shows the values for direct excitation calculated using the recommended cross-section set. The short dashed curve shows the estimated cascade contribution and the dot-dash curve shows the sum of the direct and cascade contributions. The long dashed curve shows the effective values calculated using cross-section set *C*. See text for a discussion of the three cross-section sets investigated.

els by applying the experimentally obtained branching ratios given in Ref. 22 to the calculated total excitation coefficients for the $2p$ and higher levels.[23] The results are shown by the short dashed curves in Figs. 5 and 6. The values for the total excitation coefficients, which are the sum of the direct and cascade excitations, are shown by the chain curves. The agreement between these calculated total excitation rate coefficients and experiment is good for the $1s_5$ level for all E/N. Agreement for the $1s_4$ level is poorer than for the $1s_5$ level. This will be discussed in Sec. VI.

We have checked the dependence of α_M/N on neon density, electron current, and laser intensity. The results of variation of N at several E/N are shown in Fig. 7, where the α_M/N values become independent of N at the higher densities. Possible reasons for the decrease in the apparent α_M/N values at the lower N are space-charge distortion of the electric field, contact potentials, and nonequilibrium behavior of the electrons leaving the cathode.[8] These effects are avoided in the data of Figs. 5 and 6 by operating at the higher pressures where the applied voltages are greater than about 50 V. Under typical experimental conditions the α_M/N values were found to be independent of current for an order of magnitude change in current. The estimates of uncertainties in the experiment are similar to those given in I and lead to total estimated uncertainties in the determination of α_M/N and α_R/N of $\pm 25\%$ and $\pm 35\%$, respectively.

V. BOLTZMANN ANALYSIS

We have calculated the excitation coefficients by a Boltzmann analysis in the two-term expansion approximation[24] using the computer code of Hayashi[25] in which the new electron produced by ionization is taken into account. Details of the calculational procedures are given in Ref. 24. The cross-section set most consistent with our experimental results and our recommended set is shown in Figs. 8(a) and 8(b). This will be designated as set *A*. The momentum transfer cross section was taken from Robertson[26] for energies less than 10 eV and extrapolated to 100 eV using the results of Gupta and Rees[27] for $\varepsilon \geq 100$ eV. The cross sections for the excitation of the $1s_5$, $1s_4$, $1s_3$, and $1s_2$ levels were taken from Register *et al.*[5] for $\varepsilon \geq 25$ eV. The relative values of Brunt *et al.*[28] for sums of the metastable and resonance levels near threshold were smoothly connected to the absolute values at higher energies.

The cross sections for the $2p$ levels and for higher levels

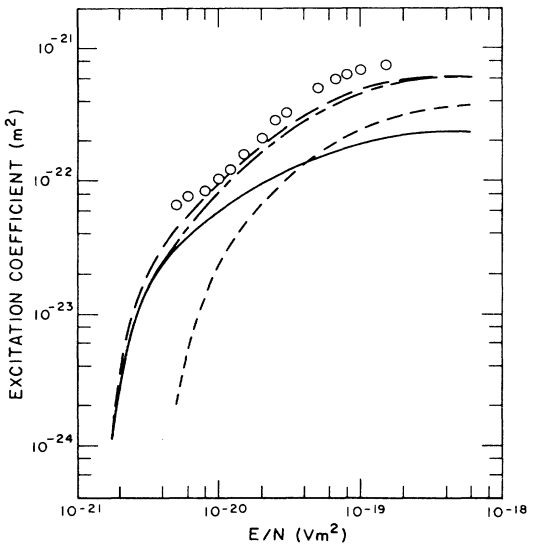

FIG. 6. Excitation coefficient α_R/N for the $1s_4$ level as a function of E/N. The meaning of the symbols and curves are the same as in Fig. 5.

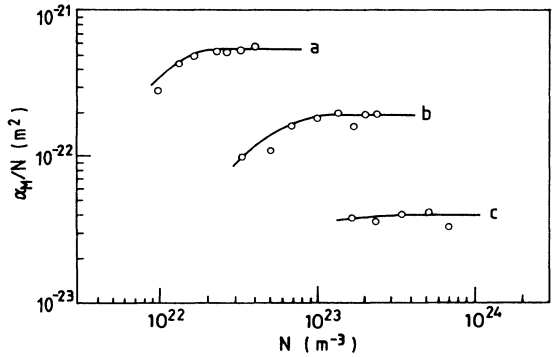

FIG. 7. Dependence of the excitation coefficient for the $1s_5$ level on the neon density for various E/N. *a*, 1×10^{-19} V m^2; *b*, 2×10^{-20} V m^2; *c*, 5×10^{-21} V m^2.

$(2s,3s,3p,3d)$ were also taken from Register *et al.*[5] for $\varepsilon \geq 25$ eV. All of the excitation cross sections were modified at higher energies to fit the total excitation cross-section data of de Heer *et al.*[29] The ionization cross section was taken from Rapp and Englander-Golden.[30] Comparison of α_M/N and α_R/N values calculated using these cross sections with experiment was discussed in Sec. IV. The calculated value of α/N for the total of the $2p$ levels agrees with the experimental value given in Ref. 22 for $E/N = 10^{-19}$ V m^2.

The cross-section set designated as set B consists of the cross sections of Phillips *et al.*[4] for the four $1s$ levels and the cross sections of set A for the remaining levels. The calculated α/N values are larger than the measured values for the $1s_5$ level and vice versa for the $1s_4$ level. When we applied scaling factors of 0.66 and 1.8 to the cross sections for the $1s_5$ and $1s_4$ levels, respectively, good agreement was obtained.[22]

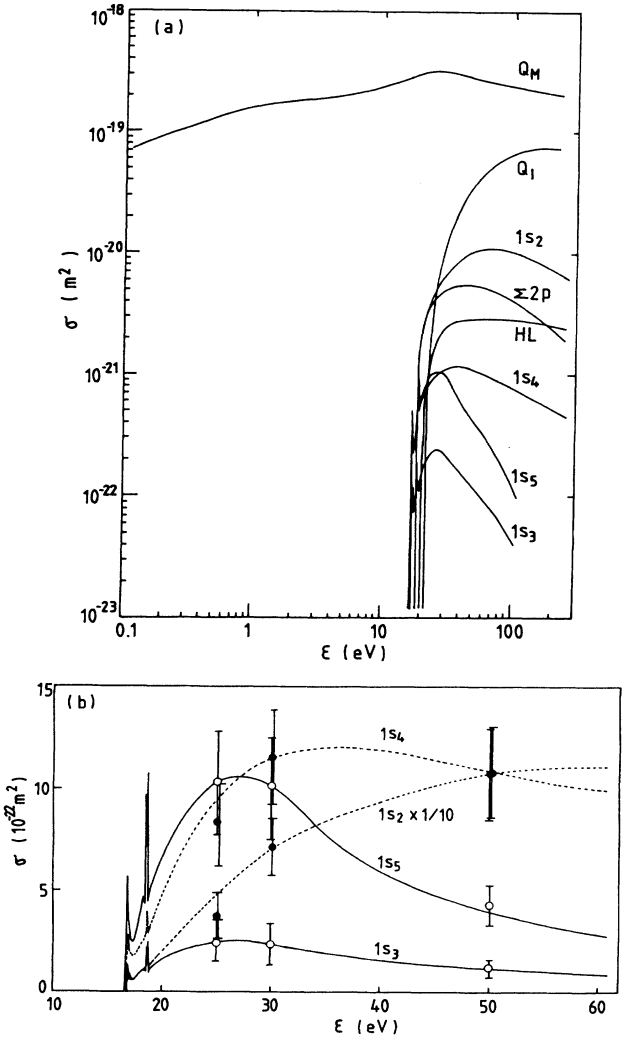

FIG. 8. (a) Recommended set of cross sections for electrons in Ne and used in Boltzmann analysis. The symbols and meanings are as follows: Q_M, momentum transfer; Q_I, ionization; $\Sigma 2p$, sum of $2p$ levels; HL, sum of higher levels. (b) Details of $1s_n$ cross sections. The points show the $1s_n$ level data from Ref. 5.

In the set of cross sections designated as set C we used the effective cross sections of Phillips *et al.*,[4] which included cascade excitation from higher levels. Therefore, no additional excitation cross sections were used. The elastic and ionization cross sections were the same as in set A. The calculated excitation coefficients are shown by the long-dashed curves of Figs. 5 and 6. The α_M/N calculated using cross-section set C are consistent with the values calculated using set B, but are larger than our measured values. On the other hand, the calculated values of α_R/N using set C fit experiment well, but are inconsistent with the values calculated with our unmodified set B. These comparisons suggest that there may be errors in the determination by Phillips *et al.*[4] of the direct cross section for electron excitation of the $1s_4$ level from their effective cross section.

Calculations using the three cross-section sets do not produce any noticeable differences in the values of the electron transport parameters, such as drift velocity and diffusion coefficient. Agreement with reported values[31] is good. However, cross-section set A produces the best agreement with experimental values[31] of α_i/N.

VI. DISCUSSION

In this section we discuss various additional factors relevant to the accuracy and interpretation of the results. Firstly, we estimate the effects of possible Penning ionization of impurities such as N_2, O_2, and H_2O by $1s$ levels. A complete model of this effect would lead to simultaneous equations for the electron and $1s_5$ and $1s_4$ level densities. Our efforts to carry out this analysis have not been completed and we have used an approximate solution in which the effects of Penning ionization of impurities are accounted for by assuming that the spatial distribution of the additional ionization is the same as that of the electron density. Penning ionization can then be accounted for by recalculating the factors Q for the electron current and the factor P for the spatial distribution of excitation. We can obtain an approximate upper limit to the effects of ionization of impurities by assuming that (a) since the $1s_5$ density is much larger than that for other levels, only ionization by $1s_5$ atoms need be considered, and (b) the fraction of the $1s_5$ atoms which lead to ionization is given by $K'_M/(K'_M+K_1)$. The effective ionization coefficient $\tilde{\alpha}_i/N$ is then given by

$$\tilde{\alpha}_i/N = (\alpha_i/N) + (\alpha_M/N)K'_M/(K'_M+K_1)\ , \qquad (20)$$

where α_i/N is the ionization coefficient for pure neon. Using the value of α_i/N tabulated in Ref. 31 and our measured values of α_M/N, the effective ionization coefficient is that shown by the chain curve of Fig. 9. The values of α_M/N and α_R/N shown in Figs. 5 and 6 include the effects of the increased α_i/N. When Penning ionization of impurities is omitted, the α_M/N and α_R/N are decreased by an amount which increases with increasing N and decreasing E/N by as much as 20%.

Another aspect which we considered was the effect of collisional mixing of the $1s_5$ and $1s_4$ levels with the $1s_3$

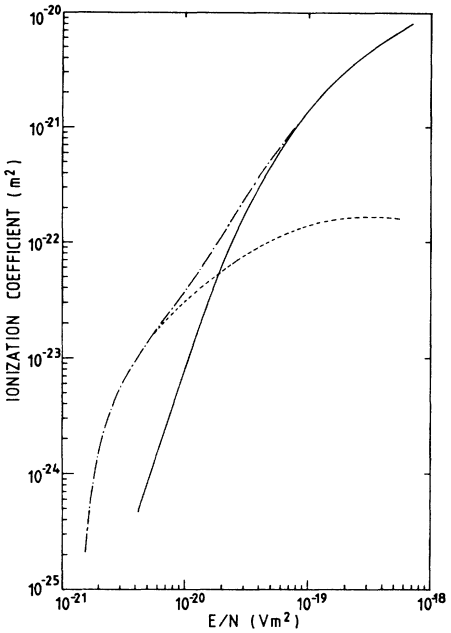

FIG. 9. Spatial ionization coefficient α_i/N as a function of E/N. The solid curve is an average of measured values from Ref. 31. The dotted curve is the estimated maximum contribution of Penning ionization of impurities for our gas samples, while the dot-dash curve is the sum of the ionization coefficients.

and $1s_2$ levels. According to the Boltzmann analysis of Sec. V, the excitation coefficient for the $1s_2$ level is large compared to those for the $1s_5$ and $1s_4$ levels. However, because of the short radiative lifetime and expected small rate coefficient for excitation transfer to the lower $1s$ levels,[15] the contribution of the $1s_2$ level to the production and loss of other $1s$ levels can be neglected. According to Ref. 15, about one-half of the $1s_3$ excitation is transferred to the $1s_4$ level and about one-half to the $1s_5$ level. However, the excitation coefficient for the $1s_3$ level obtained from our Boltzmann analysis is about 10 to 20% of those for the $1s_5$ and $1s_4$ levels, so that excitation transfer from the $1s_3$ level produces an error or less than 10% in the determination of α_M/N and α_R/N. Further support for these arguments is our observation of very small densities in the $1s_3$ and $1s_2$ levels using the absorption technique at wavelengths of 616.3 and 585.2 nm, respectively. The absorption signal for the 616.3-nm line was not detected, while the absorption signal for 585.2 nm was slightly larger than the background noise. Considering the transition probabilities for these lines and the detection limit for the present experiment, the densities of these levels are estimated to be less than or equal to 10^{11} m^{-3} when the densities of the $1s_4$ and $1s_5$ levels were of the order of 10^{12} and 10^{13} m^{-3}, respectively.

Finally, we discuss the difference between the calculated and measured values of α_R/N. If we apply a scaling factor of 1.4 to the excitation cross section for the $1s_4$ level in cross-section set A, we find a slightly better fit to the average of the experimental data. However, the dependence on E/N is less satisfactory. Such a factor appears inconsistent with the electron beam data discussed in Sec. V. Alternatively, our estimate of cascading from the $2p$ and higher levels may be too small. Thus, if we made the seemingly unrealistic assumption that about half of the cascading from $2p$ and higher levels is to the $1s_4$ level, the fit—especially the E/N dependence— is significantly improved. Other possibilities are connected with an overestimate of the excitation coefficient derived from experiment. One of these is that excitation transfer from the $1s_3$ level is more probable than estimated. However, this does not explain the discrepancy in the E/N dependence. Another possibility is that we have overestimated the effective value of ν_I so that the correct value of α_R is smaller than in Fig. 6. Thus, a decrease in ν_I to 10^4 s^{-1} results in experimental α_R/N values which average around the chain curve of Fig. 6. Evidence that the value of ν_I of 1.4×10^4 s^{-1} used in our model is correct is the agreement between calculated and experimentally derived values in Ref. 15. In addition, the calculated value of ν_I proved satisfactory in the case of Ar excitation coefficients. However, we must note that our limited and somewhat questionable[32] attempts to determine γ_i by fitting waveforms such as that of Fig. 2(b) yielded γ_i values consistent with ν_I near 10^4 s^{-1}.

VII. SUMMARY

Electron excitation coefficients have been measured for the $1s_5$ metastable and $1s_4$ resonance levels of neon at E/N from 1.6 to 300×10^{-21} V m^2 corresponding to mean electron energies from 4 to 20 eV. These coefficients have been used, along with previously published electron excitation coefficients for the $2p$ levels[22] and with electron transport and ionization coefficients,[31] to obtain a set of recommended electron excitation cross sections. These cross sections are in good agreement with the electron scattering data of Register *et al.*[5] but in less satisfactory agreement with the recent laser-induced fluorescence data of Phillips *et al.*[4]

ACKNOWLEDGMENTS

The authors wish to acknowledge helpful discussions and correspondence with L. W. Anderson, A. Gallagher, and J. L. Hall. We wish to thank Y. Urano for encouragement and support during the analysis of the results, and M. Hayashi for supplying his Boltzmann code. The experimental work and a portion of the analysis were carried out while both authors were at the Joint Institute for Laboratory Astrophysics and were supported in part by the Defense Advanced Research Projects Agency through the Office of Naval Research under Contract No. N00014-76-C123.

*Permanent address.
†Also at Quantum Physics Division, National Bureau of Standards and Department of Physics, University of Colorado.

[1]W. L. Wiese, M. W. Smith, and B. M. Glennon, *Atomic Transition Probabilities*, (U.S. Department of Commerce, Washington, D.C., 1966), Vol. 1, p. 128.
[2]K. Tachibana, Phys. Rev. A **34**, 1007 (1986).
[3]The experimental portion of this work was reported briefly earlier. See K. Tachibana and A. V. Phelps, Bull. Am. Phys. Soc. **26**, 714 (1981).
[4]M. H. Phillips, L. W. Anderson, and C. C. Lin, Phys. Rev. A **23**, 2751 (1981); M. H. Phillips, L. W. Anderson, C. C. Lin, and R. E. Miers, Phys. Lett. **82 A**, 404 (1981); R. E. Miers, J. E. Gastineau, M. H. Phillips, L. W. Anderson, and C. C. Lin, Phys. Rev. A **25**, 1185 (1982); M. H. Phillips, L. W. Anderson, and C. C. Lin, *ibid.* **32**, 2117 (1985).
[5]D. F. Register, S. Trajmar, G. Steffensen, and D. C. Cartwright, Phys. Rev. A **29**, 1793 (1984).
[6]L. E. Machado, E. P. Leal, and G. Csanak, Phys. Rev. A **29**, 1811 (1984).
[7]J. M. W. Milatz and L. S. Ornstein, Physica **2**, 355 (1935).
[8]S. A. Lawton and A. V. Phelps, J. Chem. Phys. **69**, 1055 (1978).
[9]No further purification was attempted since earlier determinations of metastable excitation coefficients showed that the effects of metastable quenching were directly accounted for by using measured decay constants and that the effects of diffusion were less important in the presence of significant quenching. However, as discussed in this paper, the presence of excited-state mixing and of Penning ionization of impurities considerably complicated the analysis of the data.
[10]J. M. Bridges and W. L. Wiese, Phys. Rev. A **2**, 285 (1970); S. Inatsugu and J. R. Holmes, *ibid.* **11**, 26 (1975).
[11]N. Van Schaik, L. W. G. Steenhuijsen, P. J. M. Van Bommel, and F. H. P. Verspaget, J. Phys. (Paris) Colloq. **7**, C-97 (1979).
[12]V. I. Odintsov, Opt. Spectrosc. (USSR) **18**, 205 (1965).
[13]G. H. Copely, J. Quant. Spectrosc. Radiat. Transfer **16**, 553 (1976).
[14]S. N. Jabr and W. R. Bennet, Jr., Phys. Rev. A **21**, 1518 (1980).
[15]A. V. Phelps, Phys. Rev. **114**, 1011 (1959).
[16]T. Holstein, Phys. Rev. **72**, 1212 (1947); **83**, 1159 (1951).
[17]N. D. Bhaskar and A. Lurio, Phys. Rev. A **13**, 1484 (1976).
[18]A. V. Phelps, Phys. Rev. A **117**, 619 (1960).
[19]P. K. Leichner, J. D. Cook, and S. J. Luerman, Phys. Rev. A **12**, 2501 (1975). The assumption of this reference that the rate coefficients of their Eqs. (10) and (14) should agree with those of their Eqs. (5) and (6) is incorrect. Using their derived rate coefficients and the corrected Eq. (A7), we find the calculated slow decay constant is a factor of 2.5 below their measurement at 4 kPa.
[20]K. Tachibana, H. Harima, and Y. Urano, Jpn. J. Appl. Phys. **21**, 1529 (1982); J. D. Clark and A. J. Cunningham, J. Phys. B **15**, 2781 (1982).
[21]A. Yokoyama and Y. Hatano, Chem. Phys. **63**, 59 (1981).
[22]K. Tachibana, H. Harima, and Y. Urano, J. Phys. B **17**, 879 (1984).
[23]It is assumed that all the excitation to levels above the $2p$ levels ($2s$, $3s$, $3d$, etc.) cascade to the $2p$ levels, i.e., the resonance transitions from the ns and nd to the ground state are effectively trapped at the Ne densities used. Collisional mixing within the cascading levels may modify the assumed branching ratios. More detailed experiment than in Ref. 18 would be required to take this effect into account. As pointed out by A. Gallagher (private communication), the contribution of cascading from the ns and nd levels becomes more important as E/N and the mean electron energy increase.
[24]L. S. Frost and A. V. Phelps, Phys. Rev. **127**, 1621 (1962). See P. E. Luft, Joint Institute for Laboratory Astrophysics (JILA) Information Center Report No. 14, 1975 (unpublished) for detailed documentation of this computer code and its modifications as of 1975.
[25]M. Hayashi (private communication). In this code the scattered electron and the new electron produced by ionization share equally the energy available after the collision. The temporal growth code described by S. Yoshida, A. V. Phelps, and L. C. Pitchford, Phys. Rev. A **27**, 2858 (1983), has been extended by S. Yoshida and A. V. Phelps (unpublished) to steady-state, spatial growth problems using the algorithms of H. Brunet and P. Vincent, J. Appl. Phys. **50**, 4700 (1980). Using this code and assuming the distribution of secondary electron energies given by C. B. Opal, W. K. Peterson, and E. C. Beaty, J. Chem. Phys. **55**, 4100 (1971), the calculated direct excitation coefficients agree with those given in Figs. 5 and 6 for $E/N = 1\times10^{-19}$ V m^2 and are 15% higher for $E/N = 5\times10^{-19}$ V m^2.
[26]A. G. Robertson, J. Phys. B **5**, 648 (1982).
[27]S. C. Gupta and J. A. Rees, J. Phys. B **8**, 417 (1975).
[28]J. N. Brunt, G. C. King, and F. H. Reed, J. Phys. B **9**, 2195 (1976); **10**, 3781 (1977).
[29]F. J. de Heer, R. H. J. Jansen, and W. van der Kaay, J. Phys. B **12**, 979 (1979).
[30]D. Rapp and P. Englander-Golden, J. Chem. Phys. **43**, 1464 (1965).
[31]J. Dutton, J. Phys. Chem. Rev. Data **4**, 577 (1975).
[32]Our measurements of γ_i are considered questionable because the associated time constants may be too close to the response time of our detection system. Further experiments would be necessary to determine accurate γ_i values.